

# Dominant contributions to the nucleon-nucleon interaction at sixth order of chiral perturbation theory

D. R. Entem,<sup>1,\*</sup> N. Kaiser,<sup>2,†</sup> R. Machleidt,<sup>3,‡</sup> and Y. Nosyk<sup>3</sup>

<sup>1</sup>*Grupo de Física Nuclear, IUFFyM, Universidad de Salamanca, E-37008 Salamanca, Spain*

<sup>2</sup>*Physik Department T39, Technische Universität München, D-85747 Garching, Germany*

<sup>3</sup>*Department of Physics, University of Idaho, Moscow, Idaho 83844, USA*

(Dated: May 15, 2015)

We present the dominant two- and three-pion-exchange contributions to the nucleon-nucleon interaction at sixth order (next-to-next-to-next-to-next-to-next-to-leading order,  $N^5\text{LO}$ ) of chiral perturbation theory. Phase shifts with orbital angular momentum  $L \geq 4$  are given parameter free at this order and allow for a systematic investigation of the convergence of the chiral expansion. The  $N^5\text{LO}$  contribution is prevalingly repulsive and considerably smaller than the  $N^4\text{LO}$  one, thus, establishing the desired trend towards convergence. Using low-energy constants that were extracted from an analysis of  $\pi N$ -scattering at fourth order, the predictions at  $N^5\text{LO}$  are in excellent agreement with the empirical phase shifts of peripheral partial waves.

PACS numbers: 13.75.Cs, 21.30.-x, 12.39.Fe, 11.10.Gh

Keywords: nucleon-nucleon scattering, chiral perturbation theory, chiral multi-pion exchange

## I. INTRODUCTION

The derivation of nuclear forces from chiral effective field theory has been a topic of active research for the past quarter century [1–17] (see also Refs. [18, 19] for recent reviews). By 1998, the evaluation of the nucleon-nucleon ( $NN$ ) interaction up to next-to-next-to-leading order ( $N^2\text{LO}$ , third order in small momenta) was completed [2–4] and, by 2003, these calculations were extended to  $N^3\text{LO}$  [5–11]. As it turned out, at  $N^2\text{LO}$  and  $N^3\text{LO}$ , one is faced with a surplus of attraction, in particular, when the low-energy constants (LECs) for subleading pion-nucleon couplings are applied consistently as extracted from analyses of elastic  $\pi N$ -scattering [3, 4, 10]. Finally, in 2014, this issue was picked up and calculations up to  $N^4\text{LO}$  were conducted [15]. It was shown that the  $2\pi$ - and  $3\pi$ -exchange contributions at  $N^4\text{LO}$  are prevalingly repulsive and, thus, are able to fully compensate the excessive attraction of the lower orders. However, it was also noticed that the  $N^2\text{LO}$ ,  $N^3\text{LO}$ , and  $N^4\text{LO}$  contributions are all roughly of the same magnitude, raising legitimate concerns about the convergence of the chiral expansion of the  $NN$ -potential.

It is, therefore, the purpose of the present paper to move on to the next order and to investigate the  $NN$ -interaction at  $N^5\text{LO}$  (of sixth power in small momenta) with the goal to obtain more insight into the convergence issue.

Besides this, the order  $N^5\text{LO}$  has other interesting features. At this order, a new set of  $NN$ -contact terms depending with the sixth power on momenta appears, bringing the total number of short-distance parameters to 50. This set includes then terms that contribute up to  $F$ -waves.

However, the focus of the present paper is on peripheral partial waves with orbital angular momentum  $L \geq 4$ , which are exclusively ruled by the non-polynomial pion-exchange expressions constrained by chiral symmetry. Hence, this investigation is a test of the implications of chiral symmetry for the  $NN$ -interaction up to sixth order.

This paper is organized as follows: In Secs. IIA, IIB, and IIC, we consider the two-, three-, and four-pion exchange contributions at sixth order and argue that some parts are negligibly small. The predictions for elastic  $NN$ -scattering in peripheral partial waves are shown in Sec. III, and Sec. IV concludes the paper.

## II. PION-EXCHANGE CONTRIBUTIONS TO THE $NN$ -INTERACTION AT $N^5\text{LO}$

This section is subdivided into three subsections in which we will consider various classes of two- and three-pion exchange diagrams. We will present arguments for neglecting the chiral four-pion exchange at this order. Our semi-analytical results will be stated in terms of contributions to the momentum-space  $NN$ -amplitudes in the center-of-mass

---

\*Electronic address: entem@usal.es

†Electronic address: nkaiser@ph.tum.de

‡Electronic address: machleidt@uidaho.edu

system (CMS), which arise from the following general decomposition of the  $NN$ -potential:

$$\begin{aligned}
V(\vec{p}', \vec{p}) = & V_C + \boldsymbol{\tau}_1 \cdot \boldsymbol{\tau}_2 W_C \\
& + [V_S + \boldsymbol{\tau}_1 \cdot \boldsymbol{\tau}_2 W_S] \vec{\sigma}_1 \cdot \vec{\sigma}_2 \\
& + [V_{LS} + \boldsymbol{\tau}_1 \cdot \boldsymbol{\tau}_2 W_{LS}] i\vec{S} \cdot (\vec{k} \times \vec{q}) \\
& + [V_T + \boldsymbol{\tau}_1 \cdot \boldsymbol{\tau}_2 W_T] \vec{\sigma}_1 \cdot \vec{q} \vec{\sigma}_2 \cdot \vec{q} \\
& + [V_{\sigma L} + \boldsymbol{\tau}_1 \cdot \boldsymbol{\tau}_2 W_{\sigma L}] \vec{\sigma}_1 \cdot (\vec{q} \times \vec{k}) \vec{\sigma}_2 \cdot (\vec{q} \times \vec{k}),
\end{aligned} \tag{2.1}$$

where  $\vec{p}'$  and  $\vec{p}$  denote the final and initial nucleon momenta in the CMS, respectively. Moreover,  $\vec{q} = \vec{p}' - \vec{p}$  is the momentum transfer,  $\vec{k} = (\vec{p}' + \vec{p})/2$  the average momentum, and  $\vec{S} = (\vec{\sigma}_1 + \vec{\sigma}_2)/2$  the total spin, with  $\vec{\sigma}_{1,2}$  and  $\boldsymbol{\tau}_{1,2}$  the spin and isospin operators, of nucleon 1 and 2, respectively. For on-shell scattering,  $V_\alpha$  and  $W_\alpha$  ( $\alpha = C, S, LS, T, \sigma L$ ) can be expressed as functions of  $q = |\vec{q}|$  and  $k = |\vec{k}|$ , only. The one-pion exchange contribution is of the well-known form  $W_T^{(1\pi)} = -(g_A/2f_\pi)^2(m_\pi^2 + q^2)^{-1}$  with  $g_A$  the axial-vector coupling constant,  $f_\pi = 92.4$  MeV the pion decay constant, and  $m_\pi$  the pion mass. Numerical values for  $g_A$  and  $m_\pi$  will be given in Sec. III. This expression fixes at the same time our sign-convention for the  $NN$ -potential  $V(\vec{p}', \vec{p})$ .

We will state contributions in terms of their spectral functions, from which the momentum-space amplitudes  $V_\alpha(q)$  and  $W_\alpha(q)$  are obtained via the subtracted dispersion integrals:

$$\begin{aligned}
V_{C,S}(q) &= \frac{2q^8}{\pi} \int_{nm_\pi}^{\tilde{\Lambda}} d\mu \frac{\text{Im } V_{C,S}(i\mu)}{\mu^7(\mu^2 + q^2)}, \\
V_T(q) &= -\frac{2q^6}{\pi} \int_{nm_\pi}^{\tilde{\Lambda}} d\mu \frac{\text{Im } V_T(i\mu)}{\mu^5(\mu^2 + q^2)},
\end{aligned} \tag{2.2}$$

and similarly for  $W_{C,S,T}$ . Clearly, the thresholds are given by  $n = 2$  for two-pion exchange and  $n = 3$  for three-pion exchange. For  $\tilde{\Lambda} \rightarrow \infty$  the above dispersion integrals yield the finite parts of loop-functions as in dimensional regularization, while for finite  $\tilde{\Lambda} \gg nm_\pi$  we employ the method known as spectral-function regularization (SFR) [20]. The purpose of the finite scale  $\tilde{\Lambda}$  is to constrain the imaginary parts to the low-momentum region where chiral effective field theory is applicable.

### A. Two-pion exchange contributions at N<sup>5</sup>LO

The  $2\pi$ -exchange contributions that occur at N<sup>5</sup>LO are displayed graphically in Fig. 1. We will now discuss each class separately.

#### 1. Spectral functions for $2\pi$ -exchange class (a)

The N<sup>5</sup>LO  $2\pi$ -exchange two-loop contributions, denoted by class (a), are shown in Fig. 1(a). For this class the spectral functions are obtained by integrating the product of the subleading one-loop  $\pi N$ -amplitude (see Ref. [21] for details) and the chiral  $\pi\pi NN$ -vertex proportional to  $c_i$  over the Lorentz-invariant  $2\pi$ -phase space. In the  $\pi\pi$  center-of-mass frame this integral can be expressed as an angular integral  $\int_{-1}^1 dx$  [8]. Altogether, the results for the non-vanishing spectral functions read:

$$\begin{aligned}
\text{Im } V_C = & \frac{m_\pi^6 \sqrt{u^2 - 4}}{(8\pi f_\pi^2)^3} \left( \frac{1}{u^2} - 2 \right) \left[ (c_2 + 6c_3)u^2 + 4(6c_1 - c_2 - 3c_3) \right] \left\{ 2c_1 u + \frac{c_2 u}{36} (5u^2 - 24) \right. \\
& + \frac{c_3 u}{2} (u^2 - 2) + \left[ c_3(2 - u^2) + \frac{c_2}{6} (4 - u^2) - 4c_1 \right] \sqrt{u^2 - 4} B(u) \left. \right\} \\
& + \frac{m_\pi^6 \sqrt{u^2 - 4}}{8\pi f_\pi^4 u} \left\{ \left[ 4c_1 + c_3(u^2 - 2) \right] \left[ \bar{e}_{15}(u^4 - 6u^2 + 8) + 6\bar{e}_{14}(u^2 - 2)^2 + \frac{3\bar{e}_{16}}{10}(u^2 - 4)^2 \right] \right. \\
& + c_2(u^2 - 4) \left[ \frac{3\bar{e}_{15}}{10}(u^4 - 6u^2 + 8) + \bar{e}_{14}(u^2 - 2)^2 + \frac{3\bar{e}_{16}}{28}(u^2 - 4)^2 \right] \left. \right\},
\end{aligned} \tag{2.3}$$

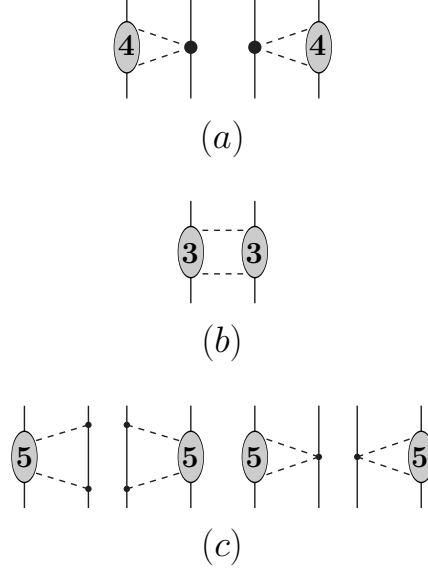


FIG. 1: Two-pion-exchange contributions to the  $NN$ -interaction at  $N^5\text{LO}$ . (a) The subleading one-loop  $\pi N$ -amplitude is folded with the chiral  $\pi\pi NN$ -vertices proportional to  $c_i$ . (b) The leading one-loop  $\pi N$ -amplitude is folded with itself. (c) The leading two-loop  $\pi N$ -amplitude is folded with the tree-level  $\pi N$ -amplitude. Solid lines represent nucleons and dashed lines pions. Small dots and large solid dots denote vertices of chiral order one and two, respectively. Shaded ovals represent complete  $\pi N$ -scattering amplitudes with their order specified by the number in the oval.

$$\begin{aligned}
\text{Im}W_S = & \frac{c_4^2 m_\pi^6 (u^2 - 4)}{9(8\pi f_\pi^2)^3} \left\{ u\sqrt{u^2 - 4} \left[ \frac{5u^2}{6} - 4 + \frac{2g_A^2}{15}(2u^2 - 23) \right] - (u^2 - 4)^2 B(u) \right. \\
& + 6g_A^2 u \int_0^1 dx \left( x - \frac{1}{x} \right) \left[ 4 + (u^2 - 4)x^2 \right]^{3/2} \ln \frac{x\sqrt{u^2 - 4} + \sqrt{4 + (u^2 - 4)x^2}}{2} \Big\} \\
& + \frac{c_4 m_\pi^6 u (u^2 - 4)^{3/2}}{240\pi f_\pi^4} \left[ 10\bar{e}_{17}(2 - u^2) + \bar{e}_{18}(4 - u^2) \right] = \mu^2 \text{Im}W_T, \tag{2.4}
\end{aligned}$$

with the dimensionless variable  $u = \mu/m_\pi > 2$  and the logarithmic function

$$B(u) = \ln \frac{u + \sqrt{u^2 - 4}}{2}. \tag{2.5}$$

Consistent with the calculation of the  $\pi N$ -amplitude in Ref. [21], we utilized the relations between the fourth-order LECs, such that only  $\bar{e}_{14}$  to  $\bar{e}_{18}$  remain in the final result.

## 2. Spectral functions for $2\pi$ -exchange class (b)

A first set of  $2\pi$ -exchange contributions at three-loop order, denoted by class (b), is displayed in Fig. 1(b). For this class of diagrams, the leading one-loop  $\pi N$ -scattering amplitude is multiplied with itself and integrated over the  $2\pi$ -phase space. Including also the symmetry factor  $1/2$ , one gets for the spectral-functions:

$$\begin{aligned}
\text{Im}V_C = & \frac{m_\pi^6 \sqrt{u^2-4}}{(4f_\pi)^8 \pi^3 u} \left\{ -\frac{3}{70}(5u^2+8)(u^2-4)^2 + 3g_A^2(1-2u^2) \left[ 1 + \frac{2-u^2}{4u} \ln \frac{u+2}{u-2} \right] \right. \\
& \times \left[ u - \frac{u^3}{2} + \frac{4B(u)}{\sqrt{u^2-4}} \right] + g_A^4 \left[ \frac{32(3-2u^2)}{\sqrt{u^2-4}} B(u) + 3(2u^2-1)^2 \left( \frac{u^2-2}{u} \ln \frac{u+2}{u-2} \right. \right. \\
& \left. \left. + \frac{(u^2-2)^2}{8u^2} \left( \pi^2 - \ln^2 \frac{u+2}{u-2} \right) \right) - \frac{2258}{35} + 24u + \frac{5336u^2}{105} - 12u^3 - \frac{2216u^4}{105} + \frac{18u^6}{35} \right] \\
& + g_A^6(2u^2-1) \left( 1 + \frac{2-u^2}{4u} \ln \frac{u+2}{u-2} \right) \left[ 46u - 3u^3 - 96 + \frac{64}{u+2} + \frac{24(5-2u^2)}{\sqrt{u^2-4}} B(u) \right] \\
& + \frac{64g_A^8}{9} \left[ \frac{3119u^2}{70} - \frac{71u^6}{1120} - \frac{197u^4}{70} - \frac{85u^3}{8} + \frac{97u}{4} - \frac{582}{7} - \frac{16}{u+2} + \frac{8}{(u+2)^2} \right. \\
& \left. \left. + \frac{6u^4 - 60u^2 + 105}{\sqrt{u^2-4}} B(u) \right] \right\}, \tag{2.6}
\end{aligned}$$

$$\begin{aligned}
\text{Im}W_S = & \frac{g_A^4 m_\pi^6 \sqrt{u^2-4}}{(4f_\pi)^8 \pi^3 u} \left\{ \frac{u^2-4}{48} \left[ 4u + (4-u^2) \ln \frac{u+2}{u-2} \right]^2 - \frac{\pi^2}{48} (u^2-4)^3 \right. \\
& + g_A^2 u \left[ (u^2-4) \ln \frac{u+2}{u-2} - 4u \right] \left[ \frac{5u}{4} - \frac{u^3}{24} - \frac{8}{3} + \frac{5-u^2}{\sqrt{u^2-4}} B(u) \right] \\
& \left. + \frac{32g_A^4 u^2}{27} \left[ \frac{u^4}{40} + \frac{13u^2}{10} + \frac{11u}{2} - \frac{118}{5} - \frac{8}{u+2} + \frac{3(10-u^2)}{\sqrt{u^2-4}} B(u) \right] \right\} = \mu^2 \text{Im}W_T, \tag{2.7}
\end{aligned}$$

$$\begin{aligned}
\text{Im}V_S = & \frac{g_A^8 m_\pi^6 u \sqrt{u^2-4}}{3(4f_\pi)^8 \pi^5} \int_0^1 dx (x^2-1) \left\{ (u^2-4)x \left[ \frac{48\pi^2 f_\pi^2}{g_A^4} (\bar{d}_{14} - \bar{d}_{15}) - \frac{1}{6} \right] + \frac{4}{x} \right. \\
& \left. - \frac{[4 + (u^2-4)x^2]^{3/2}}{x^2 \sqrt{u^2-4}} \ln \frac{x\sqrt{u^2-4} + \sqrt{4 + (u^2-4)x^2}}{2} \right\}^2 = \mu^2 \text{Im}V_T, \tag{2.8}
\end{aligned}$$

$$\begin{aligned}
\text{Im}W_C = & -\frac{m_\pi^6 (u^2-4)^{5/2}}{(4f_\pi)^8 (3\pi u)^3} \left[ 2 + 4g_A^2 - \frac{u^2}{2} (1 + 5g_A^2) \right]^2 + \frac{m_\pi^6 (u^2-4)^{3/2}}{9(4f_\pi)^8 \pi^5 u} \int_0^1 dx x^2 \left\{ \frac{3x^2}{2} (4-u^2) \right. \\
& + 3x\sqrt{u^2-4} \sqrt{4 + (u^2-4)x^2} \ln \frac{x\sqrt{u^2-4} + \sqrt{4 + (u^2-4)x^2}}{2} + g_A^4 \left[ (4-u^2)x^2 \right. \\
& \left. + 2u^2 - 4 \right] \left[ \frac{5}{6} + \frac{4}{(u^2-4)x^2} - \left( 1 + \frac{4}{(u^2-4)x^2} \right)^{3/2} \ln \frac{x\sqrt{u^2-4} + \sqrt{4 + (u^2-4)x^2}}{2} \right] \\
& + \left[ 4(1 + 2g_A^2) - u^2(1 + 5g_A^2) \right] \sqrt{u^2-4} \frac{B(u)}{u} + \frac{u^2}{6} (5 + 13g_A^2) - 4(1 + 2g_A^2) \\
& \left. \left. + 96\pi^2 f_\pi^2 \left[ (4-2u^2)(\bar{d}_1 + \bar{d}_2) + (4-u^2)x^2 \bar{d}_3 + 8\bar{d}_5 \right] \right\}^2. \tag{2.9}
\end{aligned}$$

Note the squared integrands in the last two equations. The parameters  $\bar{d}_j$  belong to the  $\pi\pi NN$ -contact vertices of third chiral order.

### 3. $2\pi$ class (c)

Further  $2\pi$ -exchange three-loop contributions at N<sup>5</sup>LO, denoted by class (c), are shown in Fig. 1(c). For these the two-loop  $\pi N$ -scattering amplitude (which is of order five) would have to be folded with the tree-level  $\pi N$ -amplitude.

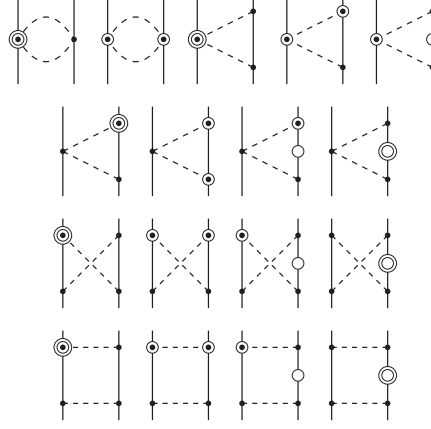


FIG. 2: Relativistic  $1/M_N^2$  corrections to  $2\pi$ -exchange diagrams that are counted as order six. Notation as in Fig. 1. Open circles represent  $1/M_N$ -corrections.

To our knowledge, the two-loop elastic  $\pi N$ -scattering amplitude has never been evaluated in some decent analytical form. Note that the loops involved in the class (c) contributions include only leading order chiral  $\pi N$ -vertices. According to our experience such contributions are typically small. For these reasons we omit class (c) in the present calculation.

#### 4. Relativistic $1/M_N^2$ -corrections

This group consists of the  $1/M_N^2$ -corrections to the chiral leading  $2\pi$ -exchange diagrams. Representative graphs are shown in Fig. 2. Since we count  $Q/M_N \sim (Q/\Lambda_\chi)^2$ , these relativistic corrections are formally of sixth order ( $N^5\text{LO}$ ). The expressions for the corresponding  $NN$ -amplitudes are adopted from Ref. [9]:

$$V_C = \frac{g_A^4}{32\pi^2 M_N^2 f_\pi^4} \left[ L(\tilde{\Lambda}; q) \left( 2m_\pi^4 + q^4 - 8m_\pi^6 w^{-2} - 2m_\pi^8 w^{-4} \right) - \frac{m_\pi^6}{2w^2} \right], \quad (2.10)$$

$$W_C = \frac{1}{192\pi^2 M_N^2 f_\pi^4} \left\{ L(\tilde{\Lambda}; q) \left[ g_A^2 \left( 2k^2 (8m_\pi^2 + 5q^2) + 12m_\pi^6 w^{-2} - 3q^4 - 6m_\pi^2 q^2 - 6m_\pi^4 \right) \right. \right. \\ \left. \left. + g_A^4 \left( k^2 (16m_\pi^4 w^{-2} - 20m_\pi^2 - 7q^2) - 16m_\pi^8 w^{-4} - 12m_\pi^6 w^{-2} + 4m_\pi^4 q^2 w^{-2} + 5q^4 + 6m_\pi^2 q^2 + 6m_\pi^4 \right) \right. \right. \\ \left. \left. + k^2 w^2 \right] - \frac{4g_A^4 m_\pi^6}{w^2} \right\}, \quad (2.11)$$

$$V_T = -\frac{1}{q^2} V_S = \frac{g_A^4 L(\tilde{\Lambda}; q)}{32\pi^2 M_N^2 f_\pi^4} \left( k^2 + \frac{5}{8} q^2 + m_\pi^4 w^{-2} \right), \quad (2.12)$$

$$W_T = -\frac{1}{q^2} W_S = \frac{L(\tilde{\Lambda}; q)}{1536\pi^2 M_N^2 f_\pi^4} \left[ g_A^4 \left( 28m_\pi^2 + 17q^2 + 16m_\pi^4 w^{-2} \right) - 2g_A^2 (16m_\pi^2 + 7q^2) + w^2 \right], \quad (2.13)$$

$$V_{LS} = \frac{g_A^4 L(\tilde{\Lambda}; q)}{128\pi^2 M_N^2 f_\pi^4} \left( 11q^2 + 32m_\pi^4 w^{-2} \right), \quad (2.14)$$

$$W_{LS} = \frac{L(\tilde{\Lambda}; q)}{256\pi^2 M_N^2 f_\pi^4} \left[ 2g_A^2 (8m_\pi^2 + 3q^2) + \frac{g_A^4}{3} \left( 16m_\pi^4 w^{-2} - 11q^2 - 36m_\pi^2 \right) - w^2 \right], \quad (2.15)$$

$$V_{\sigma L} = \frac{g_A^4 L(\tilde{\Lambda}; q)}{32\pi^2 M_N^2 f_\pi^4}, \quad (2.16)$$

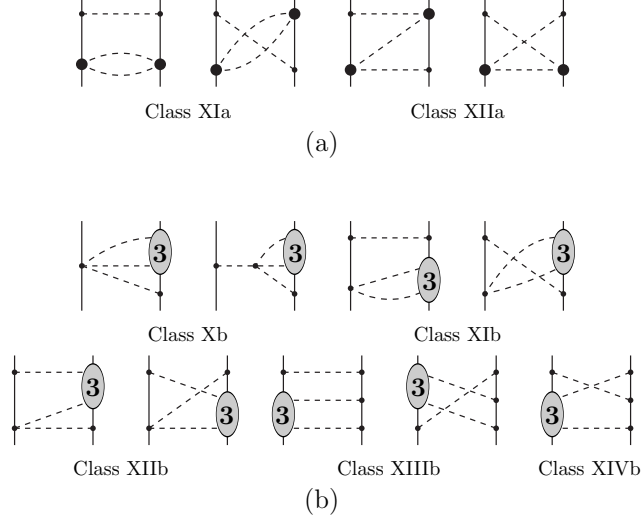


FIG. 3: Three-pion exchange contributions at  $N^5LO$ . (a) Diagrams proportional to  $c_i^2$ . (b) Diagrams involving the one-loop  $\pi N$ -amplitude. Roman numerals refer to sub-classes following the scheme introduced in Refs. [7, 15]. Notation as in Fig. 1.

where the (regularized) logarithmic loop function is given by

$$L(\tilde{\Lambda}; q) = \frac{w}{2q} \ln \frac{\tilde{\Lambda}^2(2m_\pi^2 + q^2) - 2m_\pi^2 q^2 + \tilde{\Lambda} \sqrt{\tilde{\Lambda}^2 - 4m_\pi^2} q w}{2m_\pi^2(\tilde{\Lambda}^2 + q^2)}, \quad (2.17)$$

with the abbreviation  $w = \sqrt{4m_\pi^2 + q^2}$ .

### B. Three-pion exchange contributions at $N^5LO$

The  $3\pi$ -exchange contributions of order  $N^5LO$  are shown in Fig. 3. We can distinguish between diagrams which are proportional to  $c_i^2$  [Fig. 3(a)] and contributions that involve (parts of) the leading one-loop  $\pi N$  amplitude [Fig. 3(b)]. Below, we present the spectral functions for each class.

#### 1. Spectral functions for $3\pi$ -exchange class (a)

This class consists of the diagrams displayed in Fig. 3(a). They are characterized by the presence a subleading  $\pi\pi NN$ -vertices in each nucleon line. Using a notation introduced in Refs. [7, 15], we distinguish between the various sub-classes of diagrams by roman numerals.

Class XIa:

$$\text{Im}W_C = \frac{g_A^2 c_4^2 m_\pi^6}{6(4\pi f_\pi^2)^3} \int_2^{u-1} dw (w^2 - 4)^{3/2} \sqrt{\lambda(w)}, \quad (2.18)$$

$$\begin{aligned} \text{Im}V_S = & \frac{g_A^2 c_4^2 m_\pi^6}{6(8\pi f_\pi^2)^3} \int_2^{u-1} dw \frac{(w^2 - 4)^{3/2}}{u^4 \sqrt{\lambda(w)}} \left[ w^8 - 4(1 + u^2)w^6 + 2w^4(3 + 5u^2) \right. \\ & \left. + 4w^2(2u^6 - 5u^4 - 2u^2 - 1) - (u^2 - 1)^3(5u^2 + 1) \right], \end{aligned} \quad (2.19)$$

$$\text{Im}(\mu^2 V_T - V_S) = \frac{g_A^2 c_4^2 m_\pi^6}{6(8\pi f_\pi^2)^3} \int_2^{u-1} dw (w^2 - 4)^{3/2} \sqrt{\lambda(w)} \left[ \frac{(w^2 - 1)^2}{u^4} + 1 - \frac{2}{u^2} (7w^2 + 1) \right], \quad (2.20)$$

with the kinematical function  $\lambda(w) = w^4 + u^4 + 1 - 2(w^2 u^2 + w^2 + u^2)$ . The dimensionless integration variable  $w$  is the invariant mass of a pion-pair divided by  $m_\pi$ .

Class XIIa:

$$\text{Im}V_C = \frac{g_A^2 c_4^2 m_\pi^6}{8960\pi f_\pi^6} (u-3)^3 \left[ u^3 + 9u^2 + 12u - 3 - \frac{3}{u} \right], \quad (2.21)$$

$$\text{Im}W_C = \frac{2g_A^2 c_4^2 m_\pi^6 u^2}{(4\pi f_\pi^2)^3} \iint_{z^2 < 1} d\omega_1 d\omega_2 k_1 k_2 \sqrt{1 - z^2} \arcsin(z), \quad (2.22)$$

$$\begin{aligned} \text{Im}V_S = & \frac{g_A^2 c_4^2 m_\pi^6}{(4\pi f_\pi^2)^3} \iint_{z^2 < 1} d\omega_1 d\omega_2 \left\{ 2\omega_1^2 (\omega_2^2 - 9\omega_2 u + 9u^2 + 1) + 3\omega_1 [\omega_2 (1 + 8u^2) - 6u - 6u^3] \right. \\ & + \frac{1}{4} (9u^4 + 18u^2 + 5) + \frac{2zk_2}{k_1} \left[ \omega_1^3 (4u - \omega_2) + \omega_1^2 (7\omega_2 u - 2 - 2u^2) - 2\omega_1 (2u + \omega_2) \right. \\ & \left. \left. + 2 + 2u^2 - 4\omega_2 u \right] + \frac{3 \arcsin(z)}{k_1 k_2 \sqrt{1 - z^2}} \left[ 2\omega_1^3 u (u^2 + 1 - 2\omega_2 u) + \omega_1^2 (\omega_2 u (7 + 11u^2) - 5\omega_2^2 u^2 \right. \right. \\ & \left. \left. - 1 - 4u^2 - 3u^4) + \frac{\omega_1}{4} (6u^5 + 12u^3 - 2u - \omega_2 (5 + 16u^2 + 15u^4)) + \frac{(1 - u^4)(u^2 + 3)}{8} \right] \right\}, \end{aligned} \quad (2.23)$$

$$\begin{aligned} \text{Im}(\mu^2 V_T - V_S) = & \frac{g_A^2 c_4^2 m_\pi^6}{(4\pi f_\pi^2)^3} \iint_{z^2 < 1} d\omega_1 d\omega_2 \left\{ 4\omega_1^2 (\omega_2^2 + 6u^2 + 2 - 10\omega_2 u) + 6u^2 (1 + u^2) \right. \\ & + 2\omega_1 [3\omega_2 (1 + 7u^2) - 18u^3 - 10u] + \frac{2zk_2}{k_1} \left[ \omega_1^3 (7u - 2\omega_2) + u^2 - \omega_2 u \right. \\ & \left. + \omega_1^2 (13\omega_2 u - 3 - 10u^2) + \omega_1 (2 + 3u^2)(u - 2\omega_2) \right] + \frac{3 \arcsin(z)}{k_1 k_2 \sqrt{1 - z^2}} \\ & \left. \times (u^2 - 2\omega_1 u + 1)(u^2 - 2\omega_2 u + 1) \left[ \frac{\omega_1}{2} (6u - 5\omega_2) - \frac{u^2}{2} - 2\omega_1^2 \right] \right\}, \end{aligned} \quad (2.24)$$

with the magnitudes of pion-momenta divided by  $m_\pi$ , and their scalar-product given by:

$$k_1 = \sqrt{\omega_1^2 - 1}, \quad k_2 = \sqrt{\omega_2^2 - 1}, \quad z k_1 k_2 = \omega_1 \omega_2 - u(\omega_1 + \omega_2) + \frac{u^2 + 1}{2}. \quad (2.25)$$

The upper/lower limits of the  $\omega_2$ -integration are  $\omega_2^\pm = \frac{1}{2}(u - \omega_1 \pm k_1 \sqrt{u^2 - 2\omega_1 u - 3}/\sqrt{u^2 - 2\omega_1 u + 1})$  with  $\omega_1$  in the range  $1 < \omega_1 < (u^2 - 3)/2u$ .

The contributions to  $\text{Im}W_S$  and  $\text{Im}(\mu^2 W_T - W_S)$  are split into three pieces according to their dependence on the isoscalar/isovector low-energy constants  $c_{1,3}$  and  $c_4$ :

$$\begin{aligned} \text{Im}W_S = & \frac{g_A^2 m_\pi^6 (u-3)^2}{2240\pi f_\pi^6} \left\{ 7c_1^2 \left( \frac{4}{3} + \frac{3}{u} - \frac{2}{3u^2} - \frac{1}{u^3} \right) + c_1 c_3 \left( \frac{2u^2}{3} + 4u - \frac{2}{3} \right. \right. \\ & \left. \left. - \frac{5}{u} - \frac{2}{3u^2} - \frac{1}{u^3} \right) + c_3^2 \left( \frac{3u^2}{4} + \frac{u}{8} - \frac{5}{2} - \frac{3}{u} + \frac{19}{12u^2} + \frac{19}{8u^3} \right) \right\}, \end{aligned} \quad (2.26)$$

$$\begin{aligned} \text{Im}(\mu^2 W_T - W_S) = & \frac{g_A^2 m_\pi^6 (u-3)}{1120\pi f_\pi^6} \left\{ 7c_1^2 \left( \frac{1}{3u} + \frac{1}{u^2} + \frac{3}{u^3} - 2u - 1 \right) + c_1 c_3 \left( 13u + 4 - 5u^2 - \frac{5u^3}{3} \right. \right. \\ & \left. \left. + \frac{1}{3u} + \frac{1}{u^2} + \frac{3}{u^3} \right) + \frac{c_3^2}{8} \left( 23u^2 - \frac{u^5}{3} - u^4 - 4u^3 - 8u - 3 + \frac{8}{3u} - \frac{19}{u^2} - \frac{57}{u^3} \right) \right\}, \end{aligned} \quad (2.27)$$

$$\begin{aligned} \text{Im}W_S = & \frac{g_A^2 c_4 m_\pi^6}{1120\pi f_\pi^6} (u-3)^2 \left\{ c_1 \left( u^2 + 6u - 1 - \frac{15}{2u} - \frac{1}{u^2} - \frac{3}{2u^3} \right) \right. \\ & \left. + \frac{c_3}{4} \left( \frac{2u^4}{9} + \frac{4u^3}{3} + \frac{u^2}{3} - \frac{25u}{6} + \frac{6}{u} + \frac{1}{u^2} + \frac{3}{2u^3} \right) \right\}, \end{aligned} \quad (2.28)$$

$$\begin{aligned} \text{Im}(\mu^2 W_T - W_S) = & \frac{g_A^2 c_4 m_\pi^6}{1120\pi f_\pi^6} (u-3)^3 \left\{ c_1 \left( \frac{1}{u^2} + \frac{1}{u^3} - \frac{u}{3} - 3 - \frac{4}{u} \right) \right. \\ & \left. + \frac{c_3}{4} \left( \frac{u^3}{9} + u^2 + \frac{5u}{3} + \frac{8}{3} + \frac{11}{3u} - \frac{1}{u^2} - \frac{1}{u^3} \right) \right\}, \end{aligned} \quad (2.29)$$

$$\text{Im}W_S = \frac{g_A^2 c_4^2 m_\pi^6}{8960\pi f_\pi^6} (u-3)^2 \left( \frac{25u}{12} - \frac{u^4}{9} - \frac{2u^3}{3} - \frac{u^2}{6} - \frac{3}{u} - \frac{1}{2u^2} - \frac{3}{4u^3} \right), \quad (2.30)$$

$$\text{Im}(\mu^2 W_T - W_S) = \frac{g_A^2 c_4^2 m_\pi^6}{8960\pi f_\pi^6} (u-3)^3 \left( \frac{1}{2u^2} + \frac{1}{2u^3} - \frac{u^3}{18} - \frac{u^2}{2} - \frac{5u}{6} - \frac{4}{3} - \frac{11}{6u} \right). \quad (2.31)$$

## 2. Spectral functions for $3\pi$ -exchange class (b)

This class is displayed in Fig. 3(b). Each  $3\pi$ -exchange diagram of this class includes the one-loop  $\pi N$ -amplitude (completed by the low-energy constants  $\bar{d}_j$ ). Only those parts of the  $\pi N$ -scattering amplitude, which are either independent of the pion cms-energy  $\omega$  or depend on it linearly could be treated with the techniques available. The contributions are, in general, small. Below, we present only the larger portions within this class. The omitted pieces are about one order of magnitude smaller. To facilitate a better understanding, we have subdivided this class into sub-classes labeled by roman numerals, following Refs. [7, 15].

The auxiliary function

$$\begin{aligned} G(w) = & \left[ 1 + 2g_A^2 - \frac{w^2}{4}(1 + 5g_A^2) \right] \frac{\sqrt{w^2 - 4}}{w} \ln \frac{w + \sqrt{w^2 - 4}}{2} \\ & + \frac{w^2}{24} (5 + 13g_A^2) - 1 - 2g_A^2 + 48\pi^2 f_\pi^2 \left[ (2 - w^2)(\bar{d}_1 + \bar{d}_2) + 4\bar{d}_5 \right], \end{aligned} \quad (2.32)$$

arises from the part linear in  $\omega$  of the isovector non-spin-flip  $\pi N$ -amplitude  $g^-(\omega, t)$  with  $t = (wm_\pi)^2$  (see e.g. Appendix B in Ref. [21]). The spectral functions derived from this selected set of  $3\pi$ -exchange diagrams read as follows.

Class Xb:

$$\text{Im}W_S = \frac{g_A^2 m_\pi^6}{(4f_\pi)^8 \pi^5} \int_2^{u-1} dw \frac{4G(w)}{27w^2 u^4} \left[ (w^2 - 4)\lambda(w) \right]^{3/2}, \quad (2.33)$$

$$\text{Im}(\mu^2 W_T - W_S) = \frac{g_A^2 m_\pi^6}{(4f_\pi)^8 \pi^5} \int_2^{u-1} dw \frac{4G(w)}{9w^2 u^4} (w^2 - 4)^{3/2} \sqrt{\lambda(w)} \frac{3u^2 + 1}{u^2 - 1} \left[ u^4 - (w^2 - 1)^2 \right]. \quad (2.34)$$



Class XIIb:

$$\text{Im}W_S = \frac{g_A^2 m_\pi^6}{(4f_\pi)^8 \pi^5} \int_2^{u-1} dw \frac{8G(w)}{27w^2 u^4} (w^2 - 4)^{3/2} \sqrt{\lambda(w)} \left[ 2u^2(1 + 7w^2) - u^4 - (w^2 - 1)^2 \right], \quad (2.35)$$

$$\text{Im}(\mu^2 W_T - W_S) = \frac{g_A^2 m_\pi^6}{(4f_\pi)^8 \pi^5} \int_2^{u-1} dw \frac{8G(w)}{9w^2 u^4} \frac{(w^2 - 4)^{3/2}}{\sqrt{\lambda(w)}} (u^2 + 1 - w^2)^2 \left[ 2w^2(1 + 3u^2) - w^4 - (u^2 - 1)^2 \right]. \quad (2.36)$$

Class XIIIb:

$$\text{Im}W_S = \frac{g_A^2 m_\pi^6}{9f_\pi^8 (4\pi)^5} \iint_{z^2 < 1} d\omega_1 d\omega_2 G(w) \left[ (\omega_1^2 + \omega_2^2 - 2)(1 - 3z^2) - 5k_1 k_2 z \right], \quad (2.37)$$

$$\text{Im}(\mu^2 W_T - W_S) = -\frac{g_A^2 m_\pi^6}{3f_\pi^8 (4\pi)^5} \iint_{z^2 < 1} d\omega_1 d\omega_2 G(w) \omega_1 \omega_2 \left[ 5 + 2z \left( \frac{k_1}{k_2} + \frac{k_2}{k_1} \right) \right], \quad (2.38)$$

setting  $w = \sqrt{1 + u^2 - 2u\omega_1}$ .

Class XIIIb:

$$\text{Im}V_S = \frac{g_A^4 m_\pi^6}{(4f_\pi)^8 \pi^3 u^3} \int_2^{u-1} dw 2G(w) \lambda(w) (2 - w^2), \quad (2.39)$$

$$\text{Im}(\mu^2 V_T - V_S) = \frac{g_A^4 m_\pi^6}{(4f_\pi)^8 \pi^3 u^3} \int_2^{u-1} dw 4G(w) (2 - w^2) (1 + u^2 - w^2)^2, \quad (2.40)$$

$$\begin{aligned} \text{Im}W_S = & \frac{g_A^4 m_\pi^6}{3f_\pi^8 (4\pi)^5} \iint_{z^2 < 1} d\omega_1 d\omega_2 G(w) \left\{ u(\omega_1 + 4\omega_2) - 2 - \frac{\omega_1^2 + 8\omega_2^2}{3} + z^2(\omega_1^2 + 4\omega_2^2 - 5) \right. \\ & \left. + \frac{zk_2}{k_1} (4u\omega_1 + \omega_1^2 - 5) + \frac{zk_1}{k_2} (u\omega_2 + \omega_2^2 - 2) + \frac{\arcsin(z)}{\sqrt{1 - z^2}} \left[ \frac{k_1}{k_2} (1 - u\omega_2) + z(1 - u\omega_1) \right] \right\}, \end{aligned} \quad (2.41)$$

$$\begin{aligned} \text{Im}(\mu^2 W_T - W_S) = & \frac{g_A^4 m_\pi^6}{f_\pi^8 (4\pi)^5} \iint_{z^2 < 1} d\omega_1 d\omega_2 \frac{2\omega_1}{3} G(w) \left\{ \frac{2\omega_2}{k_1^2} [\omega_1(u - \omega_2) - 1] + u + 2\omega_2 \right. \\ & \left. + \frac{zk_1\omega_2}{k_2} + \frac{zk_2}{k_1} (4u + \omega_1) + \omega_1 \left( \frac{2zk_2}{k_1} \right)^2 + \frac{\arcsin(z)}{k_1 k_2 \sqrt{1 - z^2}} \left[ (1 + u^2) \left( \omega_1 + \omega_2 - \frac{u}{2} \right) - 2u\omega_1\omega_2 \right] \right\}, \end{aligned} \quad (2.42)$$

setting again  $w = \sqrt{1 + u^2 - 2u\omega_1}$ .

Class XIVb:

$$\text{Im}V_S = \frac{g_A^4 m_\pi^6}{(4f_\pi)^8 \pi^3 u^3} \int_2^{u-1} dw \frac{G(w)}{2} \lambda(w) \left[ u^2 + w^2 + 4(u^2 - 1)w^{-2} - 5 \right], \quad (2.43)$$

$$\text{Im}(\mu^2 V_T - V_S) = \frac{g_A^4 m_\pi^6}{(4f_\pi)^8 \pi^3 u^3} \int_2^{u-1} dw G(w) (w^2 - 1 - u^2) \left[ w^4 - 2w^2(3 + u^2) + (u^2 - 1)^2(1 + 4w^{-2}) \right]. \quad (2.44)$$

### C. Four-pion exchange at N<sup>5</sup>LO

The exchange of four pions between two nucleons occurs for the first time at N<sup>5</sup>LO. The pertinent diagrams involve three loops and only leading order vertices, which explains the sixth power in small momenta. Three-pion exchange with just leading order vertices turned out to be negligibly small [5, 6], and so we expect four-pion exchange with leading order vertices to be even smaller. Therefore, we can safely neglect this contribution.

TABLE I: Low-energy constants as determined in Ref. [21]. The sets ‘GW’ and ‘KH’ are based upon the  $\pi N$  partial wave analyses of Refs. [26] and [27], respectively. The  $c_i$ ,  $\bar{d}_i$ , and  $\bar{e}_i$  are in units of  $\text{GeV}^{-1}$ ,  $\text{GeV}^{-2}$ , and  $\text{GeV}^{-3}$ .

	GW	KH
$c_1$	-1.13	-0.75
$c_2$	3.69	3.49
$c_3$	-5.51	-4.77
$c_4$	3.71	3.34
$\bar{d}_1 + \bar{d}_2$	5.57	6.21
$\bar{d}_3$	-5.35	-6.83
$\bar{d}_5$	0.02	0.78
$\bar{d}_{14} - \bar{d}_{15}$	-10.26	-12.02
$\bar{e}_{14}$	1.75	1.52
$\bar{e}_{15}$	-5.80	-10.41
$\bar{e}_{16}$	1.76	6.08
$\bar{e}_{17}$	-0.58	-0.37
$\bar{e}_{18}$	0.96	3.26

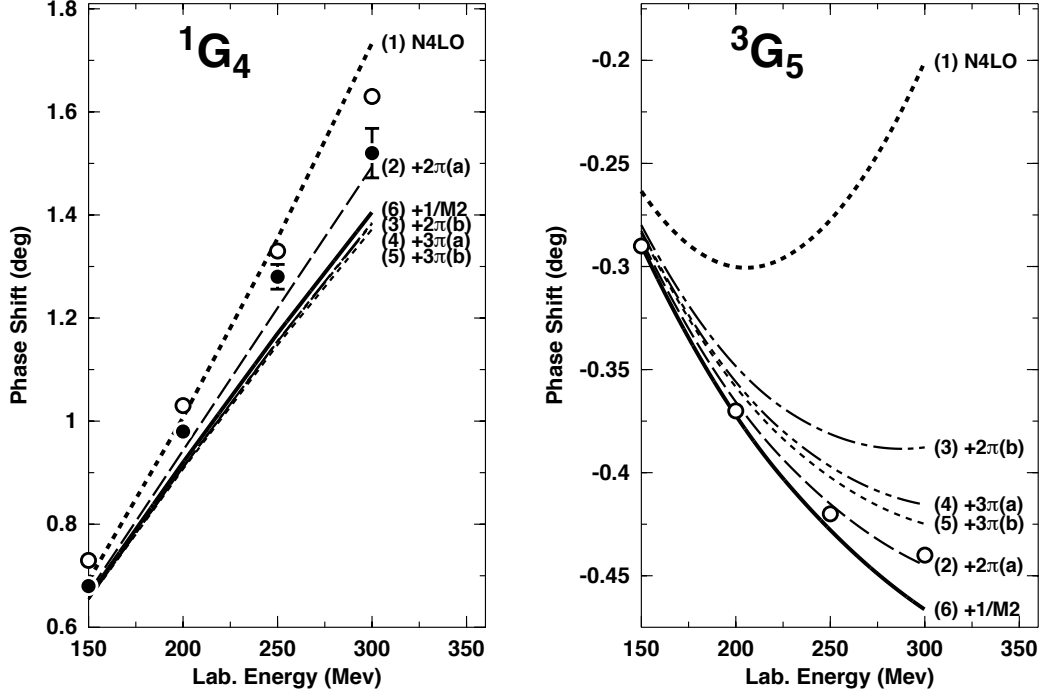


FIG. 4: Effect of individual sixth-order contributions on the neutron-proton phase shifts of two important  $G$ -waves. The individual contributions are added up successively in the order given in parentheses next to each curve. Curve (1) is  $N^4\text{LO}$  and curve (6) contains all  $N^5\text{LO}$  contributions calculated in this work. A SFR cutoff  $\tilde{\Lambda} = 900$  MeV is applied. The filled and open circles represent the results from the Nijmegen multi-energy  $np$  phase-shift analysis [28] and the GWU  $np$ -analysis SP07 [29], respectively.

### III. PERTURBATIVE $NN$ -SCATTERING IN PERIPHERAL PARTIAL WAVES

To obtain an idea of the physical relevance and implications of the contributions evaluated in Sec. II, we will now calculate the impact of these on elastic  $NN$ -scattering in peripheral partial waves. Specifically, we will consider partial waves with orbital angular momentum  $L \geq 4$  (i.e.,  $G$ -waves and higher), because polynomial terms up to sixth power do not make any contributions to these angular momentum states. The  $L \geq 4$  partial waves are sensitive only to the

non-polynomial pion-exchange expressions governed by chiral symmetry.

The smallness of the phase-shifts in peripheral partial waves suggests that the calculation can be done perturbatively. This avoids the complications and possible model-dependences (e.g., cutoff-dependence) that the non-perturbative treatment with the Lippmann-Schwinger equation, necessary for low partial waves, is beset with.

Previous systematic investigations of peripheral partial waves have been conducted at N<sup>2</sup>LO in Refs. [3, 4], at N<sup>3</sup>LO in Ref. [10], and at N<sup>4</sup>LO in Ref. [15]. Here, we will now present the investigation at N<sup>5</sup>LO.

The perturbative  $K$ -matrix for neutron-proton ( $np$ ) scattering is calculated as follows:

$$K(\vec{p}', \vec{p}) = V_{1\pi}^{(np)}(\vec{p}', \vec{p}) + V_{2\pi, \text{it}}^{(np)}(\vec{p}', \vec{p}) + V(\vec{p}', \vec{p}) \quad (3.1)$$

with  $V_{1\pi}^{(np)}(\vec{p}', \vec{p})$  the one-pion-exchange (1PE) potential that applies to  $np$  scattering taking charge-dependence into account. It is given by

$$V_{1\pi}^{(np)}(\vec{p}', \vec{p}) = -V_{1\pi}(m_{\pi^0}) + (-1)^{I+1} 2 V_{1\pi}(m_{\pi^\pm}), \quad (3.2)$$

where  $I = 0, 1$  denotes the total isospin of the  $pn$ -system and

$$V_{1\pi}(m_\pi) = -\frac{g_A^2}{4f_\pi^2} \frac{\vec{\sigma}_1 \cdot \vec{q} \vec{\sigma}_2 \cdot \vec{q}}{q^2 + m_\pi^2}. \quad (3.3)$$

We use the values  $m_{\pi^0} = 134.9766$  MeV and  $m_{\pi^\pm} = 139.5702$  MeV for the neutral and charged pion mass.  $V_{2\pi, \text{it}}^{(np)}(\vec{p}', \vec{p})$  represents the once-iterated 1PE given by:

$$V_{2\pi, \text{it}}^{(np)}(\vec{p}', \vec{p}) = \mathcal{P} \int \frac{d^3 p''}{(2\pi)^3} \frac{M_N^2}{E_{p''}} \frac{V_{1\pi}^{(np)}(\vec{p}', \vec{p}'') V_{1\pi}^{(np)}(\vec{p}'', \vec{p})}{p^2 - p''^2}, \quad (3.4)$$

where  $\mathcal{P}$  denotes the principal value and  $E_{p''} = \sqrt{M_N^2 + p''^2}$ . At sixth order, up to three iterations of  $1\pi$ -exchange should be included. However, we found that the difference between the once-iterated 1PE and the infinitely-iterated 1PE is so small that it could not be identified on the scale of our phase shift figures. For that reason, we omit iterations of 1PE beyond what is contained in  $V_{2\pi, \text{it}}^{(np)}(\vec{p}', \vec{p})$ .

Finally, the third term on the right hand side of Eq. (3.1),  $V(\vec{p}', \vec{p})$ , stands for the sum of irreducible multi-pion exchange contributions that occur at the order up to which the calculation is conducted. In multi-pion exchanges, we use the average pion mass  $m_\pi = 138.039$  MeV and, thus, neglect the charge-dependence due to pion-mass splitting. For the average nucleon mass, we use twice the reduced mass of the  $pn$ -system:

$$M_N = \frac{2M_p M_n}{M_p + M_n} = 938.9183 \text{ MeV}. \quad (3.5)$$

Through relativistic kinematics, the CMS on-shell momentum  $p$  is related to the kinetic energy  $T_{\text{lab}}$  of the incident neutron in the laboratory system, by:

$$p^2 = \frac{M_p^2 T_{\text{lab}} (T_{\text{lab}} + 2M_n)}{(M_p + M_n)^2 + 2T_{\text{lab}} M_p}, \quad (3.6)$$

with  $M_p = 938.2720$  MeV and  $M_n = 939.5654$  MeV the proton and neutron masses, respectively. The  $K$ -matrix, Eq. (3.1), is decomposed into partial waves following Ref. [22] and phase-shifts  $\delta_L$  are then calculated via

$$\tan \delta_L(T_{\text{lab}}) = -\frac{M_N^2 p}{16\pi^2 E_p} p K_L(p, p). \quad (3.7)$$

For more details concerning the evaluation of phase shifts, including the case of coupled partial waves, see Ref. [23] or the appendix of Ref. [24].

Chiral symmetry establishes a link between the dynamics in the  $\pi N$ -system and the  $NN$ -system (through common low-energy constants). In order to check the consistency, we use the LECs for subleading  $\pi N$ -couplings as determined in analyses of low-energy elastic  $\pi N$ -scattering. Appropriate analyses for our purposes are contained in Refs. [21, 25], where  $\pi N$ -scattering has been calculated at fourth order using the same power-counting of relativistic  $1/M_N$ -corrections as in the present work. Ref. [21] performed two fits, one to the GW [26] and one to the KH [27] partial wave analysis resulting in the two sets of LECs listed in Table I. In our present work, we apply the GW set unless

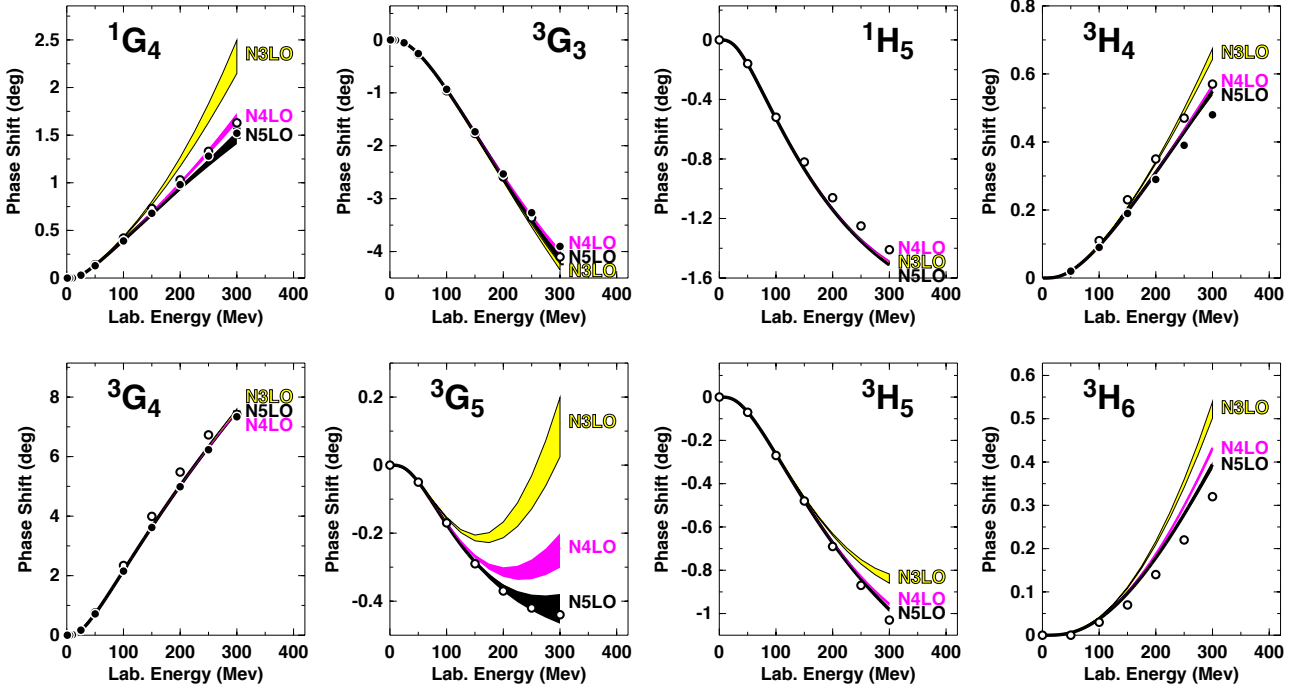


FIG. 5: (Color online) Phase-shifts of neutron-proton scattering in  $G$  and  $H$  waves at various orders as denoted. The shaded (colored) bands show the variations of the predictions when the SFR cutoff  $\tilde{\Lambda}$  is changed over the range 700 to 900 MeV. Empirical phase shifts are as in Fig. 4.

noted otherwise. Moreover, we absorb the Goldberger-Treiman discrepancy into an effective value of the nucleon axial-vector coupling constant  $g_A = g_{\pi NN} f_\pi / M_N = 1.29$ .

As shown in Figs. 1 to 3 and derived in Sec. II, the sixth-order corrections consists of several contributions. We will now demonstrate how the individual sixth-order contributions impact  $NN$ -phase-shifts in peripheral waves. For this purpose, we display in Fig. 4 phase-shifts for two important peripheral partial waves, namely,  $^1G_4$ , and  $^3G_5$ . In each frame, the following curves are shown:

- (1)  $N^4\text{LO}$  (as defined in Ref. [15]).
- (2) The previous curve plus the  $N^5\text{LO}$   $2\pi$ -exchange contributions of class (a), Fig. 1(a) and Sec. II A 1.
- (3) The previous curve plus the  $N^5\text{LO}$   $2\pi$ -exchange contributions of class (b), Fig. 1(b) and Sec. II A 2.
- (4) The previous curve plus the  $N^5\text{LO}$   $3\pi$ -exchange contributions of class (a), Fig. 3(a) and Sec. II B 1.
- (5) The previous curve plus the  $N^5\text{LO}$   $3\pi$ -exchange contributions of class (b), Fig. 3(b) and Sec. II B 2.
- (6) The previous curve plus the  $1/M_N^2$ -corrections (denoted by ‘ $1/M^2$ ’), Fig. 2 and Sec. II A 4.

In summary, the various curves add up successively the individual  $N^5\text{LO}$  contributions in the order indicated by the curve labels. The last curve in this series, curve (6), includes all  $N^5\text{LO}$  contributions calculated in this paper. For all curves of this figure a SFR cutoff  $\tilde{\Lambda} = 900$  MeV [cf. Eq. (2.2)] is employed.

From Fig. 4, we make the following observations. The two-loop  $2\pi$ -exchange class (a), Fig. 1(a), generates a strong repulsive central force through the spectral function Eq. (2.3), while the spin-spin and tensor forces provided by this class, Eq. (2.4), are negligible. The fact that this class produces a relatively large contribution is not unexpected, since it is proportional to  $c_i^2$ . The  $2\pi$ -exchange contribution class (b), Fig. 1(b), creates a moderately repulsive central force as seen by its effect on  $^1G_4$  and a noticeable tensor force as the impact on  $^3G_5$  demonstrates. The  $3\pi$ -exchange class (a), Fig. 3(a), is negligible in  $^1G_4$ , but noticeable in  $^3G_5$  and, therefore, it should not be neglected. This contribution is proportional to  $c_i^2$ , which suggests a non-negligible size but it is typically smaller than the corresponding  $2\pi$ -exchange contribution class (a). The  $3\pi$ -exchange class (b) contribution, Fig. 3(b), turns out to be negligible [see the difference between curve (4) and (5) in Fig. 4]. This may not be unexpected since it is a three-loop contribution with only

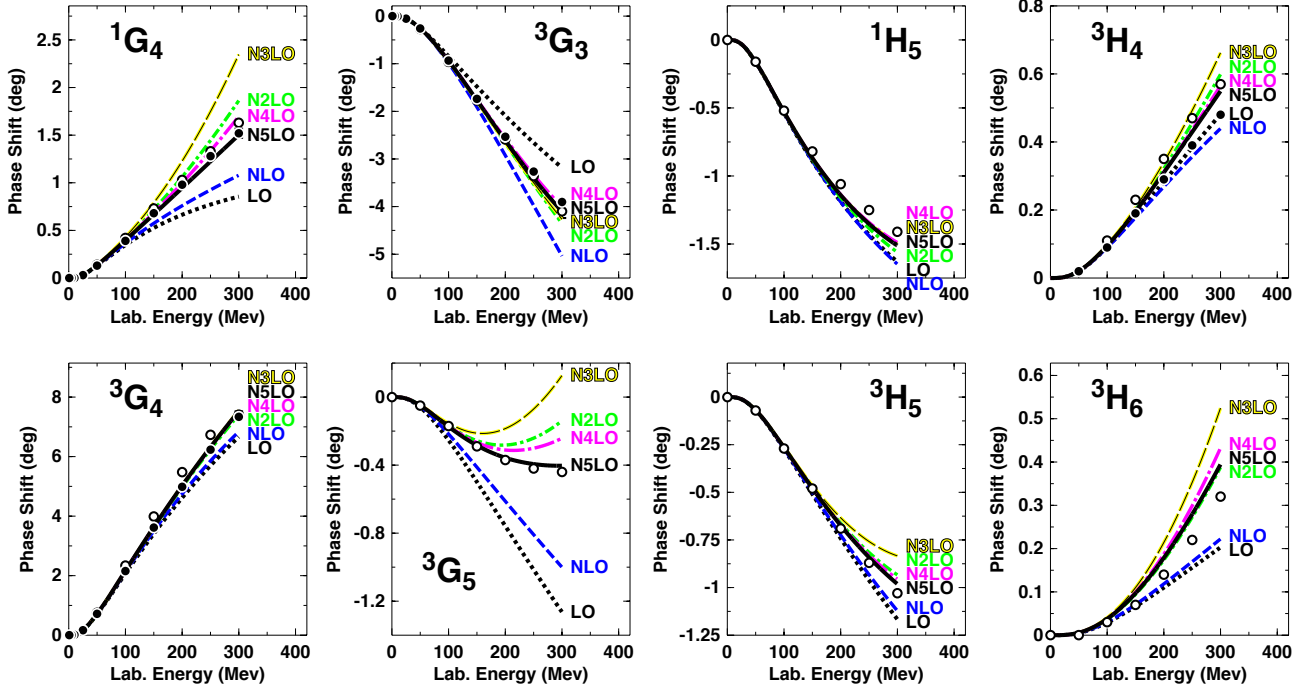


FIG. 6: (Color online) Phase-shifts of neutron-proton scattering in  $G$  and  $H$  waves at all orders from LO to  $N^5$ LO. A SFR cutoff  $\tilde{\Lambda} = 800$  MeV is used. Empirical phase shifts are as in Fig. 4.

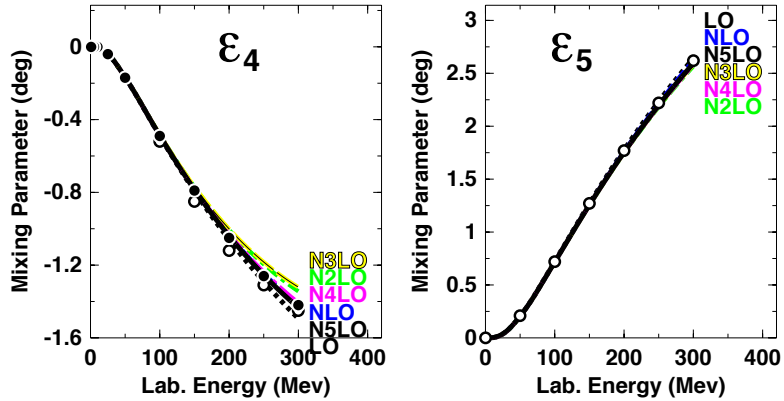


FIG. 7: (Color online) Mixing angles for neutron-proton scattering for  $J = 4, 5$  at all orders from LO to  $N^5$ LO. A SFR cutoff  $\tilde{\Lambda} = 800$  MeV is used. Filled and open circles are as in Fig. 4.

leading-order vertices. Finally the relativistic  $1/M_N^2$ -corrections to the leading  $2\pi$ -exchange, Fig. 2, have a small but non-negligible impact, particularly in  $^3G_5$ .

The predictions for all  $G$  and  $H$  waves, are displayed in Fig. 5 in terms of shaded (colored) bands that are generated by varying the SFR cutoff  $\tilde{\Lambda}$  [cf. Eq. (2.2)] between 700 and 900 MeV. The figure clearly reveals that, at  $N^3$ LO, the predictions are, in general, too attractive. As demonstrated in Ref. [15], the  $N^4$ LO contribution, essentially, compensates this attractive surplus. Now, let us turn to the new result at  $N^5$ LO: it shows a moderate repulsive contribution bringing the final prediction right onto the data (i.e. empirical phase-shifts). Moreover, the  $N^5$ LO contribution is, in general, substantially smaller than the one at  $N^4$ LO, thus, establishing a clear signature of convergence of the chiral expansion.

At this point a comment is in place concerning the empirical phase shifts with which we compare our predictions in Figs. 4 to 8. We use the 1993 Nijmegen analysis [28] (represented by filled circles in the figures) and the GWU analysis

from summer 2007 [29] (open circles). We have also considered the recent Granada  $NN$ -analysis [30]. However, it turned out that, in general, the Granada and Nijmegen analyses are so close to each other that it does not make sense to show them separately. Concerning a second analysis, we decided for GWU [29] for two reasons. The GWU analysis is truly alternative to Nijmegen (and Granada), because it is not performed with a cleaned-up data base; it uses the full  $NN$ -data base. Moreover, the GWU analysis provides empirical phase shifts also for partial waves with  $J = 5, 6$ , which we need. (The Nijmegen and Granada analyses stop at  $J = 4$ .)

Figure 5 includes only the three highest orders. However, a comparison between all orders is also of interest. Therefore, we show in Figs. 6 the contributions to phase shifts through all six chiral orders from LO to  $N^5\text{LO}$  (as defined in Ref. [15] and the present paper). Note that the difference between the LO prediction (one-pion-exchange, dotted line) and the data (filled and open circles) is to be provided by two- and three-pion exchanges, i.e. the intermediate-range part of the nuclear force. How well that is accomplished is a crucial test for any theory of nuclear forces. NLO produces only a small contribution, but  $N^2\text{LO}$  creates substantial intermediate-range attraction (most clearly seen in  $^1G_4$ ,  $^3G_5$ , and  $^3H_6$ ). In fact,  $N^2\text{LO}$  is the largest contribution among all orders. This is due to the one-loop  $2\pi$ -exchange (2PE) triangle diagram which involves one  $\pi\pi NN$ -contact vertex proportional to  $c_i$ . This vertex represents correlated 2PE as well as intermediate  $\Delta(1232)$ -isobar excitation. It is well-known from the traditional meson theory of nuclear forces [31–33] that these two features are crucial for a realistic and quantitative 2PE model. Consequently, the one-loop  $2\pi$ -exchange at  $N^2\text{LO}$  is attractive and assumes a realistic size describing the intermediate-range attraction of the nuclear force about right. At  $N^3\text{LO}$ , more one-loop 2PE is added by the bubble diagram with two  $c_i$ -vertices, a contribution that seemingly is overestimating the attraction. This attractive surplus is then compensated by the prevalingly repulsive two-loop  $2\pi$ - and  $3\pi$ -exchanges that occur at  $N^4\text{LO}$  and  $N^5\text{LO}$ .

In this context, it is worth to note that also in conventional meson theory [31] the one-loop models for the 2PE contribution always show some excess of attraction (cf. Figs. 7-9 of Ref. [10]). The same is true for the dispersion theoretic approach pursued by the Paris group [32, 33]. In conventional meson theory, the surplus attraction is reduced by heavy-meson exchange ( $\rho$ - and  $\omega$ -exchange) which, however, has no place in chiral effective field theory (as a finite-range contribution). Instead, in the latter approach, two-loop  $2\pi$ - and  $3\pi$ -exchanges provide the corrective action.

We now turn to Figs. 7, where we show how the six chiral orders impact the mixing angles with  $J = 4, 5$ . Note that the mixing angles depend only on the tensor force (the quadratic spin-orbit term  $V_{\sigma L}$  in Eq.(2.16) is very small). It is clearly seen that the  $1\pi$ -exchange (LO) alone describes these mixing angles correctly and that the various higher orders make only negligible contributions, particularly, for  $J = 5$ . At any order in the chiral expansion, tensor forces are created, but obviously the tensor force contributions beyond LO are of shorter range such that they do not matter in peripheral waves with  $L \geq 4$ .

In Figs. 4 to 7 we employed the GW set of  $\pi N$  LECs (cf. Table I). Since these LECs carry some uncertainty [25], it is of interest to know what alternative sets will predict. In Fig. 8 we show phase-shift predictions for the KH set and compare them to those from the GW set. It is seen that the differences are moderate and that both sets provide an about equally good description of the peripheral partial waves.

#### IV. CONCLUSIONS

In this paper, we have calculated dominant  $2\pi$ - and  $3\pi$ -exchange contributions to the  $NN$ -interaction which occur at  $N^5\text{LO}$  (sixth order) of the chiral low-momentum expansion. The calculations are done in heavy-baryon chiral perturbation theory using the most general fourth order Lagrangian for pions and nucleons. We apply low-energy constants for subleading  $\pi N$ -coupling, which were determined from an analysis of elastic  $\pi N$ -scattering to fourth order using the same power counting scheme as in the present work. The spectral functions, which determine the  $NN$ -amplitudes via subtracted dispersion integrals, are regularized by a cutoff  $\tilde{\Lambda}$  in the range 0.7 to 0.9 GeV. Besides the cutoff  $\tilde{\Lambda}$ , our calculations do not involve any adjustable parameters.

Recent work on  $NN$ -scattering in chiral perturbation theory [15], had revealed that the  $N^2\text{LO}$ ,  $N^3\text{LO}$ , and  $N^4\text{LO}$  contributions are all about of the same size, thus raising some concern about the convergence of the chiral expansion for the  $NN$ -potential. Our present calculations show that the contribution at  $N^5\text{LO}$  is substantially smaller than the one at  $N^4\text{LO}$ , thus, establishing a clear signature of convergence. The two-loop  $2\pi$ -exchange contribution is the largest, while the corresponding three-loop contribution is small, but not negligible. Three-pion exchange is generally small at this order. The phase-shift predictions in  $G$  and  $H$  waves, where only the non-polynomial terms governed by chiral symmetry contribute, are in excellent agreement with the data.

This investigation represents the most comprehensive (and successful) test of the implications of chiral symmetry for the  $NN$ -system.

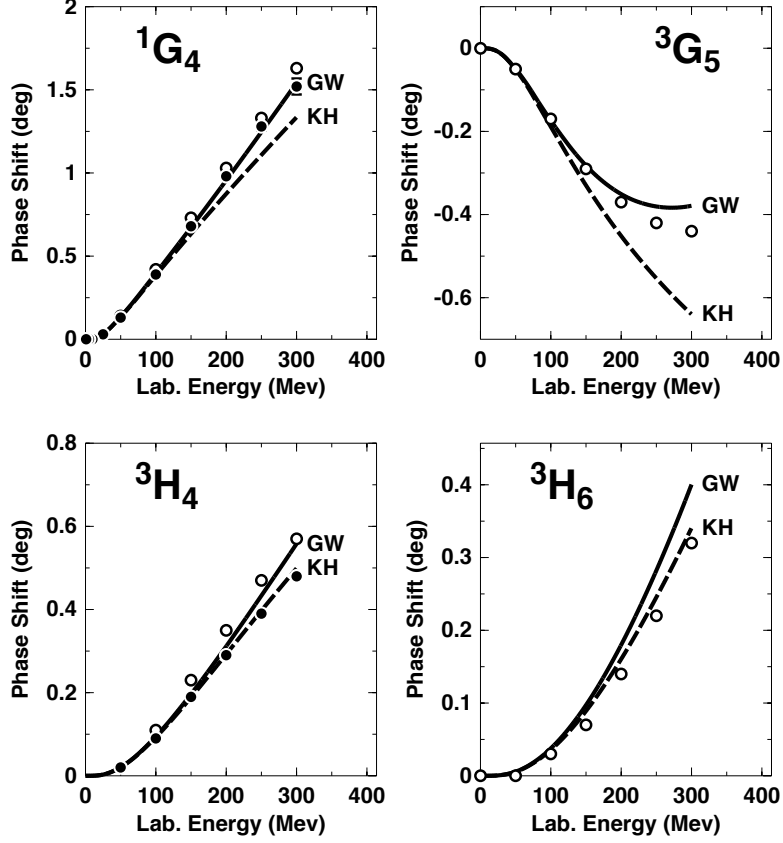


FIG. 8: Neutron-proton phase shifts for some important  $G$  and  $H$  waves using the GW and the KH sets of  $\pi N$  LECs, as denoted. A SFR cutoff  $\tilde{\Lambda} = 700$  MeV is used. Empirical phase shifts are as in Fig. 4.

### Acknowledgements

This work was supported in part by the U.S. Department of Energy under Grant No. DE-FG02-03ER41270 (R.M. and Y.N.), the Ministerio de Ciencia y Tecnología under Contract No. FPA2010-21750-C02-02 and the European Community-Research Infrastructure Integrating Activity “Study of Strongly Interacting Matter” (HadronPhysics3 Grant No. 283286) (D.R.E.), and by DFG and NSFC (CRC110) (N.K.).

- 
- [1] S. Weinberg, Phys. Lett **B251**, 288 (1990); Nucl. Phys. **B363**, 3 (1991).
  - [2] C. Ordóñez, L. Ray, and U. van Kolck, Phys. Rev. Lett. **72**, 1982 (1994); Phys. Rev. C **53**, 2086 (1996).
  - [3] N. Kaiser, R. Brockmann, and W. Weise, Nucl. Phys. **A625**, 758 (1997).
  - [4] N. Kaiser, S. Gerstendörfer, and W. Weise, Nucl. Phys. **A637**, 395 (1998).
  - [5] N. Kaiser, Phys. Rev. C **61**, 014003 (1999).
  - [6] N. Kaiser, Phys. Rev. C **62**, 024001 (2000).
  - [7] N. Kaiser, Phys. Rev. C **63**, 044010 (2001).
  - [8] N. Kaiser, Phys. Rev. C **64**, 057001 (2001).
  - [9] N. Kaiser, Phys. Rev. C **65**, 017001 (2001).
  - [10] D. R. Entem and R. Machleidt, Phys. Rev. C **66**, 014002 (2002).
  - [11] D. R. Entem and R. Machleidt, Phys. Rev. C **68**, 041001 (2003).
  - [12] E. Epelbaum, W. Glöckle, and U.-G. Meißner, Nucl. Phys. **A637**, 107 (1998); **A671**, 295 (2000).
  - [13] E. Epelbaum, W. Glöckle, and U.-G. Meißner, Nucl. Phys. **A747**, 362 (2005).
  - [14] A. Ekström, G. Baardsen, C. Forssen, G. Hagen, M. Hjorth-Jensen, G. R. Jansen, R. Machleidt, W. Nazarewicz, T. Papenbrock, J. Sarich, and S. M. Wild, Phys. Rev. Lett. **110**, 192502 (2013).

- [15] D. R. Entem, N. Kaiser, R. Machleidt, and Y. Nosyk, Phys. Rev. C **91**, 014002 (2015).
- [16] M. Piarulli, L. Girlanda, R. Schiavilla, R. Navarro Perez, J. E. Amaro and E. Ruiz Arriola, Phys. Rev. C **91**, 024003 (2015).
- [17] N. Kaiser, “Three-pion exchange nucleon-nucleon potentials with virtual  $\Delta$ -isobar excitation,” arXiv:1504.05131 [nucl-th].
- [18] R. Machleidt and D. R. Entem, Phys. Rep. **503**, 1 (2011).
- [19] E. Epelbaum, H.-W. Hammer, and U.-G. Meißner, Rev. Mod. Phys. **81**, 1773 (2009).
- [20] E. Epelbaum, W. Glöckle, and U.-G. Meißner, Eur. Phys. J. A **19**, 125 (2004).
- [21] H. Krebs, A. Gasparyan, and E. Epelbaum, Phys. Rev. C **85**, 054006 (2012). We thank H. Krebs for pointing out and clarifying misprints in this paper.
- [22] K. Erkelenz, R. Alzetta, and K. Holinde, Nucl. Phys. **A176**, 413 (1971).
- [23] R. Machleidt, in: *Computational Nuclear Physics 2 – Nuclear Reactions*, edited by K. Langanke, J.A. Maruhn, and S.E. Koonin (Springer, New York, 1993) p. 1.
- [24] R. Machleidt, Phys. Rev. C **63** 024001 (2001).
- [25] K. A. Wendt, B. D. Carlsson, and A. Ekström, “Uncertainty Quantification of the Pion-Nucleon Low-Energy Coupling Constants up to Fourth Order in Chiral Perturbation Theory,” arXiv:1410.0646 [nucl-th].
- [26] R. A. Arndt, W. J. Briscoe, I. I. Strakovsky, and R. L. Workman, Phys. Rev. C **74**, 045205 (2006).
- [27] R. Koch, Nucl. Phys. A **448**, 707 (1986).
- [28] V. G. J. Stoks, R. A. M. Klomp, M. C. M. Rentmeester, and J. J. de Swart, Phys. Rev. C **48**, 792 (1993).
- [29] W. J. Briscoe, I. I. Strakovsky, and R. L. Workman, SAID Partial-Wave Analysis Facility, Data Analysis Center, The George Washington University, solution SP07 (Spring 2007).
- [30] R. Navarro Perez, J. E. Amaro and E. Ruiz Arriola, Phys. Rev. C **88**, 064002 (2013).
- [31] R. Machleidt, K. Holinde, and Ch. Elster, Phys. Rep. **149** (1987) 1.
- [32] R. Vinh Mau, in: *Mesons in Nuclei*, Vol. I, edited by M. Rho and D. H. Wilkinson (North-Holland, Amsterdam, 1979), p. 151.
- [33] M. Lacombe, B. Loiseau, J. M. Richard, R. Vinh Mau, J. Côté, P. Pires, and R. de Tournell, Phys. Rev. C **21** (1980) 861.